Performance and Hub Vibrations of an Articulated Slowed-Rotor Compound Helicopter at High Speeds

Jean-Paul Reddinger
Ph.D. Student
Rensselaer Polytechnic Institute
Troy, NY

Farhan Gandhi
Professor
Rensselaer Polytechnic Institute
Troy, NY

Hao Kang
Research Engineer
US Army Research Laboratory
Aberdeen Proving Ground, MD

ABSTRACT

For a compound helicopter with an articulated main rotor, this study focuses on the high advance ratio, low disk loading environment of high speed flight at 225 kts. It seeks to understand the predominant phenomena which contribute to the main rotor power and hub vibrations, and demonstrate the most sensitive design and control criteria used in minimizing them for steady level flight—specifically the use of redundant controls and the effect of blade twist. The compound model is based on a UH-60A with 20,110 lbs of gross weight, and simulations are performed by Rotorcraft Comprehensive Analysis Sytem. The results show that for a -8° twisted rotor, the minimum power and minimum vibration states exist for two distinct sets of redundant controls and main rotor behavior. The low power state occurs at lower RPM and higher auxiliary thrust, with lower flapping and thrust at the main rotor. At a state with reduced vibrations, main rotor forward tilt, thrust, and average inflow ratio are higher, such that the rear of the rotor encounters less of the wake from the preceding rotor blades. For an untwisted rotor, it is shown that the regions for minimum power and minimum vibrations coincide with each other, with almost no flapping or pitch inputs and reduced rotor thrust from the twisted blade. By untwisting the rotor and providing proper control settings, the power requirements can be reduced by about 4–7%, with potential reductions in hub vibrations ranging from 50–80%.

NOTATION

S_x	sectional blade drag in rotating reference frame
S_z	sectional blade lift in rotating reference frame
T_P	twisted rotor, trim state at low power
T_V	twisted rotor, trim state with low vibrations
U_P	untwisted rotor, trim state at low power
U_V	untwisted rotor, trim state with low vibrations

INTRODUCTION

The maximum speed capability of conventional rotary-wing aircraft (with rotors operating edgewise in forward flight) is 150–170 kts, limited by the onset of compressibility effects on the advancing blade tip, stall on the retreating side of the rotor disk, high vibration, and deterioration in rotor performance leading to an eventual inability to produce the required forces. Tilting the rotors forward to function as propellers and transferring the lifting function to the wing is one approach to overcome these challenges. While they can attain maximum speeds in excess of 275 kts, tiltrotor aircraft like the V22-Osprey have a significantly higher empty-weight fraction, increased complexity, and reduced hover and low-speed performance (Ref. 1). If the maximum speed requirement is in the 200–250 kt range, lift-offset coaxial configurations and slowed rotor compound configurations with auxiliary lift and propulsion may well be more viable solutions, offering reduced complexity and improved hover performance relative to tiltrotor aircraft. Coaxial rotor technology, using two counter-rotating rotors with each of the rotors generating lift on its advancing side in the high-speed regime, was referred to as the Advancing Blade Concept and first implemented on the Sikorsky XH-59 helicopter in the 1970's (Ref. 2). After a hiatus of several years, Sikorsky Aircraft Corp. developed a second generation high-speed coaxial rotor aircraft prototype, the X2 Technology Demonstrator (Refs. 3–6), which improved on many of the shortcomings of the XH-59. The X2 technologies are being scaled up for application to the S-97 Raider, and to the SB>1 Defiant, the latter in response to the Army's JMR program (Refs. 7, 8).

Lift-offset coaxial configurations use auxiliary propulsion at high speeds, but with each rotor generating lift on the advancing side they eschew the need for a lifting wing. Like their coax counterparts, slowed-rotor compound helicopters also use auxiliary propulsion in high-speed, but transfer most of the lifting function to wings and therefore operate at a reduced rotor disk loading. Efforts focused on the development of slowed rotor compound configurations go back several decades with the AH-56 Cheyenne representing a significant milestone (Ref. 9). More recently, designs for a Large Civil Tandem Compound were pursued under the NASA Joint Heavy Lift Program (Ref. 10), while Piasecki Aircraft Corp. developed and demonstrated their Vectored Thrust Ducted Propeller (VTDP) system on a compounded X-49A Speed-

Presented at the AHS 71st Annual Forum, Virginia Beach, Virginia, May 5–7, 2015.

Hawk aircraft (Ref. 11). In 2010 Airbus Helicopters unveiled their X^3 demonstrator (Ref. 12), which compounded the airframe of the AS 365 Dauphin with a lifting wing and five-bladed tractor propellers at the wing tips. It has since set the current speed record of 255 kts for an edgewise rotor in level flight.

In addition to the major design and development programs discussed above, many fundamental studies over the years have focused on the performance and benefits of compound helicopters (Refs. 13–22). To contribute to understanding of the aeromechanical behavior of slowed-rotors in high speed flight, a series of wind tunnel experiments were conducted on UH-60A rotors at high advance ratios under the NASA/Army UH-60A Airloads Program (Ref. 23). By supplementing the classical helicopter controls with control of the rotor RPM, wing flaps and ailerons, elevators, and auxiliary thrust, a compound helicopter provides an opportunity to exploit control redundancy and fly the aircraft in any number of different ways. For example, the controls could be selected to minimize the power requirement, vibrations, blade flapping, acoustic noise, or some weighted combination thereof, while satisfying vehicle force and moment equilibrium in steady level flight (Refs. 24–28), or to improve handling qualities in maneuvering flight (Ref. 29). Sekula and Gandhi have demonstrated the vibration reduction capabilities of compounding a hingeless rotor with fixed system auxiliary forces at moderate speeds (Refs. 24–26).

In a recent effort, Horn and co-workers (Refs. 30, 31) attempted to determine the optimal control configurations of a high-speed compound aircraft in-flight, using Fly-to-Optimal methods. The approach, based on perturbation of individual controls, requires a substantial amount of time, especially when multiple redundant controls are used, and the solution is itself dependent on the sequence of control perturbations. While the Fly-to-Optimal approach makes no use of any prior knowledge of the system in attempting to determine the best compound helicopter controls, Reddinger and Gandhi (Ref. 32) focused on a physics-based approach to arrive at and understand the optimal trim states. The study in Ref. 32, based on a compound derivative of a modified UH-60A Black Hawk helicopter operating in the range of 225–250 kts, focused primarily on power minimization, while considering constraints on controls, rotor flapping, etc. The current study extends the effort of Ref. 32 to examine the use of additional controls to minimize power requirements and hub vibrations of an offloaded, articulated rotor in high speed flight, with consideration to additional attributes such as the effect of blade twist. The simulations are based on the use of the US Army's Rotorcraft Comprehensive Analysis System (RCAS) (Ref. 33).

COMPOUND HELICOPTER MODELING AND ANALYSIS

Figure 1 illustrates the fully compounded model with emphasis on relevant subsystems and the dominant aerodynamic forces. The figure defines the reference planes and terminology to be used throughout the paper. The rotor drag is defined as parallel to the wind axis, and the rotor lift is the force vector opposite gravity. In the tip path reference plane—which tilts longitudinally and laterally due to blade flapping—the rotor thrust is orthogonal to the tip path plane. The rotor H-force is defined as the vector perpendicular to the thrust, in the same plane as both the thrust and the wind axis.

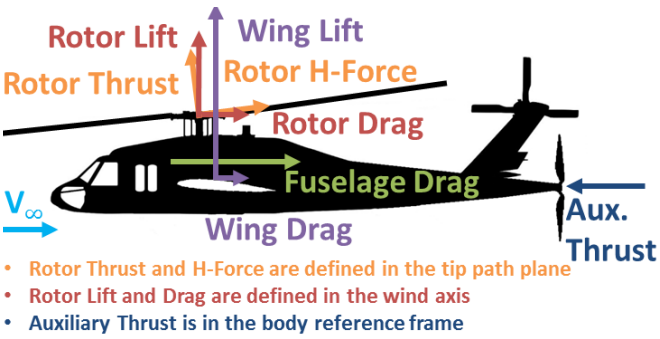

Fig. 1. Free body diagram of compound configuration with dominant aerodynamic forces labeled

The compound helicopter model used in the simulations of this study is adapted from a UH-60A rotor and fuselage model. Table 1 provides a summary of the compound configuration's major subsystems and their characteristics. Auxiliary thrust is to be provided for high-speed flight, so the forward shaft tilt present on the UH-60A is removed. Furthermore, while the UH-60A twist provides excellent hover performance, the large non-linear twist at the tip results in high negative lift and drag at the advancing blade tips for high advance ratios. For the present study, a more moderate -8° twist is considered and further compared against an untwisted rotor. Other features of the UH-60A rotor including airfoil selections, chord distribution, and sectional mass and stiffness properties are left unchanged. The airfoil aerodynamic coefficients are interpolated from nonlinear lookup tables.

The gross takeoff weight is increased to 20,110 lbs, which is equivalent to the takeoff weight of the Piasecki X-49A SpeedHawk. This increased weight can be assumed to include the weight of the wings, propulsor, and any additional weight required to compound the UH-60A airframe. To model fuselage drag, the compounded fuselage is assumed to be more streamlined than the UH-60A fuselage. A UH-60A has a minimum equivalent flat plate drag area of 35.14 ft^2 (Ref. 34). According to trends established by Ormiston (Ref. 19), a modern aircraft at this gross weight that is designed for high speed flight can be expected to have an equivalent flat plate drag area of 18.49 ft^2. The quadratic relation between vehicle pitch attitude and drag as measured for the UH-60A was maintained, resulting in the following expression for the equivalent flat plate drag area as a function of vehicle pitch (in degrees).

$$f_D = 18.487 + 0.0441\alpha^2 \ (\text{ft}^2)$$

The wing model is based on the three dimensional lift,

Table 1. Compound helicopter configuration

Characteristic	Measurement
Gross Weight	20,110 lbs
C.G. Location	1.5 ft aft, 5.8 ft below hub
Main Rotor	
Rotor Radius	26.8 ft
Nominal Rotor Speed	258 RPM
Nominal Blade Twist	-8°
Shaft Tilt	0°
Airfoils	SC-1094 R8/SC-1095
Horizontal Stabilizer	
Effective Area	43 ft^2
Pitch Angle	0.4°
Airfoil	NACA 0012
Wing	
Planform Area	220 ft^2
Chord	5 ft
Wingspan	44 ft
Incidence Angle	3.8°
Aerodynamic Properties	Aerostar FJ-100
C.P. Location	0.5 ft aft, 6.5 ft below hub
Propulsor	
Radius	5.2 ft
Speed	1,474 RPM
Solidity	0.12
Efficiency	0.85–0.86
Location	33.7 ft aft, 5.8 ft below hub

drag, and moment coefficients for the wing of the Aerostar FJ-100, which is the wing used on the X-49A. It has been set at an incidence of 3.8°, so that for pitch-level flight at 225 kts it will be flying close its peak L/D of 22.4, and scaled in area from 178.2 ft^2 to 220 ft^2 so that at this attitude it will be lifting about 83% of the gross weight of the aircraft. With only 1.2° of nose-up vehicle pitch, the wings can produce enough aerodynamic lift to completely offset the aircraft weight, and will still be operating at an L/D of 21.2.

The auxiliary thrust is modeled as a point force acting parallel to the waterline of the aircraft, in line with the center of gravity, and 1.16 ft behind the tail rotor. The magnitude of the thrust is prescribed as a control, and any resultant torque is assumed to be offset by the ailerons (Ref. 32) at a negligible increase in wing drag. Propulsor power is determined using a blade element vortex theory (BEVT) model of a seven-bladed propeller with a 5.2 ft radius at 1,474 RPM, which gives a propeller efficiency of 0.85–0.86 for the range of thrusts considered in this study.

The horizontal stabilizer is modeled after the size and location of the UH-60A stabilizer, with airfoil coefficients interpolated from a table of NACA 0012 wind tunnel data. Since this study focuses on high-speed operation of 225 kts, it is assumed that the wake of the main rotor is swept away, and does not interfere with the free stream velocity at the stabilizer. The pitch of the stabilizer is set to 0.4° with respect to the waterline of the aircraft. This was determined to be within a tenth of a degree of the best setting for each case considered in this study, which will keep the pitch of the aircraft level, offload most of the lifting function to the wings, and trim close to minimal power (Ref. 32).

A dual core prescribed wake model is selected to calculate the inflow, which captures the effects of producing negative lift on the advancing tip of the blade, and the resulting second vortex inboard of the tip vortex. Offloaded main rotors operate at a low collective pitch, resulting in the generation of more negative lift at the advancing tip than is generally seen in conventional helicopters. Therefore, it is of greater importance for an offloaded compound helicopter to model not only the tip vortex, but the second vortex inboard of the tip.

The structural and aerodynamic models are built to the above mentioned specifications in RCAS (Ref. 33), using 13 elastic beam elements, 36 aerodynamic sections, and an azimuthal resolution of 5° for calculation of airloads. The flap and lag hinges, and pitch bearings are modeled as torsional spring/damper elements, and pitch control is prescribed through a spring element with a stiffness that is representative of the pitch link and swashplate stiffness of a UH-60A. As a computational tool, RCAS has been independently validated against wind tunnel data of an untwisted H-34 rotor at advance ratios up to 0.46 using a prescribed wake model (Ref. 35).

For a fully compounded helicoter, there can exist up to eleven trim variables: the four conventional pilot controls, aircraft pitch and roll attitude, main rotor speed, auxiliary thrust, horizontal stabilizer pitch, wing collective flaps, and wing differential flaps. The collective flaps have the same effect of increasing wing lift share as a combination of wing incidence and horizontal stabilizer pitch, which have been set to achieve this end. With wing differential flap prescribed such that their roll moments counter the torque of the propulsor (based on the findings of Ref. 32), three of the five redundant controls are no longer free variables. Trim analyses are performed at 225 kts using conventional trim variables (the four conventional pilot controls, pitch and roll attitudes). The remaining redundant controls—rotor speed and prescribed auxiliary thrust—are swept from 178–224 RPM, and from 4400–4860 lbs, respectively.

TWISTED BLADE RESULTS

To examine the ability of additional control settings to improve the performance of a compound helicopter in high speed, forces and moments are equilibrated at 225 kts to determine the conventional controls required to trim a rotor with a -8° linearly twisted blade. Parametric variations in auxiliary thrust and rotor speed are performed to find the settings that produce the lowest states of power requirements and vibratory force levels. Contour maps for the ranges of trim states are provided in Figures 2 and 3. The contours are plotted against variations in auxiliary thrust on the x-axis, and in % reduction from the nominal rotor speed (258 RPM) on the y-axis. Figure 2 represent the total vehicle power, which is the sum of the main rotor power and the propulsor power. Figure 3 shows the variation in total magnitude of the 4/rev hub vibratory force levels (in g). The total magnitude is resolved from

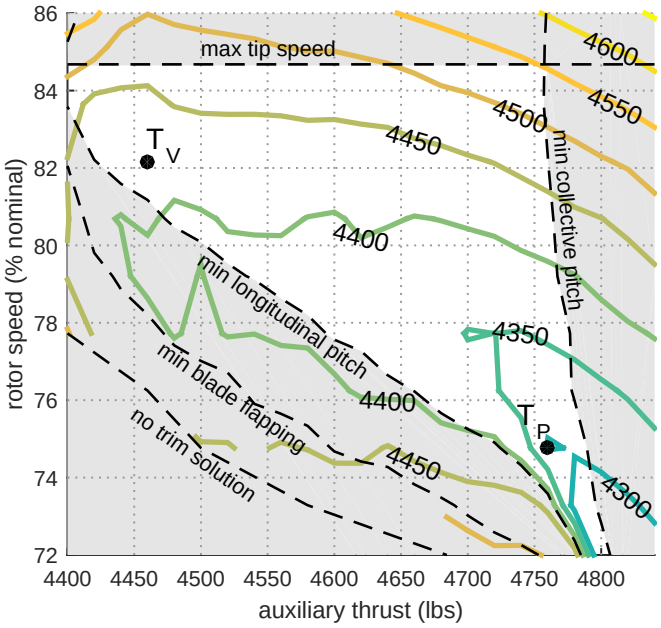

Fig. 2. Map of total power (hp) for the twisted blade

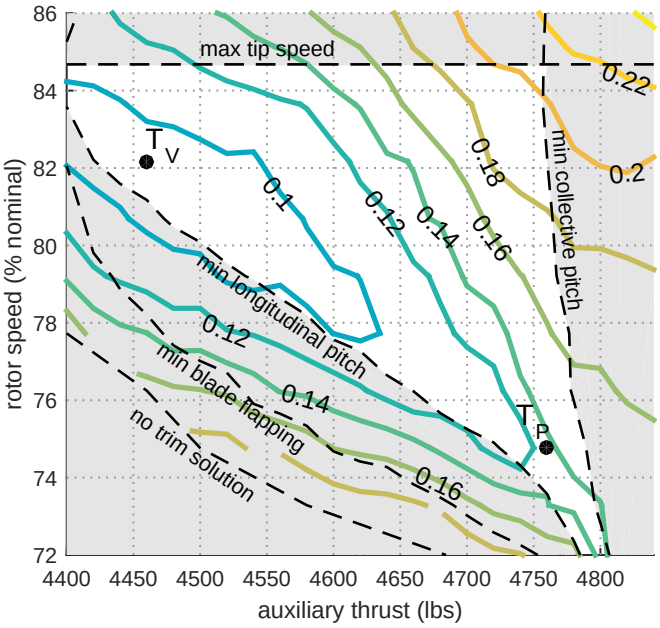

Fig. 3. Map of total 4/rev vibratory hub forces (g) for the twisted blade

the longitudinal, lateral and vertical components of vibration, which have been mapped separately in Figures 4, 5, and 6. Total 4/rev vibratory hub moments (presented as accelerations) are also considered in Figure 7. Bounds for minimum collective pitch input, longitudinal pitch input, and minimum blade flapping are marked based on the stick travel and flapping limits of the conventional UH-60A rotor, which are summarized in Table 2. An additional rotor speed constraint is placed so that the advancing tip does not exceed Mach 0.89.

Table 2. Main rotor control and flapping limits

Rotor Condition	Limits
Collective Pitch	$0.4^\circ \leq \theta_{75} \leq 16.4^\circ$
Lateral Pitch	$-8^\circ \leq \theta_{1c} \leq 8^\circ$
Longitudinal Pitch	$-16^\circ \leq \theta_{1s} \leq 16^\circ$
Blade Flapping	$-6^\circ \leq \beta_{\text{min}} \leq 22^\circ$
Adv. Tip Mach No.	$M_{\text{tip}} \leq 0.89$
Rotor Speed	RPM $\leq$ 218 (84.7% nom.)

In the region on the bottom left corner of the map, the auxiliary thrust is insufficient to overcome the total aircraft drag, requiring large longitudinal pitch inputs to tilt the rotor forward and use a component of the main rotor thrust to overcome a portion of the main rotor drag force (Ref. 32). In Figure 2, the minimum longitudinal pitch boundary shows where longitudinal pitch requirements exceed the defined pitch control bounds—signifying that the main rotor is incapable of tilting as far as is required by the auxiliary thrust deficit. As auxiliary thrust increases, rotor blade flapping and longitudinal pitch inputs decrease. Since the lifting function is primarily on the wings, the main rotor in the feasible region operates with very low disk loading, and the collective pitch setting is also very low. For very high auxiliary thrusts, the main rotor thrust is reduced so far that the collective pitch violates its minimum bound, as shown on the right hand side of Figure 2.

Rotor speed is limited on the upper end by the maximum tip speed, above which compressibility effects and drag divergence result in a drop in performance. As RPM is reduced the rotor advance ratio increases, and the dynamic pressures outside of the reverse flow region decrease, resulting in less total rotor thrust for constant pitch inputs. In order to equilibrate the longitudinal rotor forces with the rest of the longitudinal vehicle forces, the reduced component of thrust in the tip path plane must be tilted forward by a larger angle, so the longitudinal blade pitch input and flap response must increase. The result on the map is that as rotor speed decreases, the lower bound of feasibility for auxiliary thrust as limited by minimum longitudinal pitch moves to larger values.

Trim for Low Power

Comparing Figures 2, 3, and 7 shows that the trim states for best performance and for minimal vibrations do not coincide, but occupy two distinct regions. For comparison, a low power case from Figure 2 and a low vibration case from Figures 3 and 7 are selected. These trim states are labeled T_P and T_V, respectively, and are detailed in Table 3. T_V is at low auxiliary thrust and higher rotor speed with respect to T_P. Moving from T_V to T_P reduces the total power of the vehicle from 4415 hp to 4298 hp, of which the rotor power is nearly halved, from 801 hp to 402 hp, while the propulsor power increases with auxiliary thrust from 3614 hp to 3896 hp.

The higher power case, T_V, is used as a baseline to demonstrate the mechanics of T_P that result in a power reduction. T_V is trimmed with 4460 lbs of auxiliary thrust and a 212 RPM rotor speed, which is 82% of the nominal operating speed of

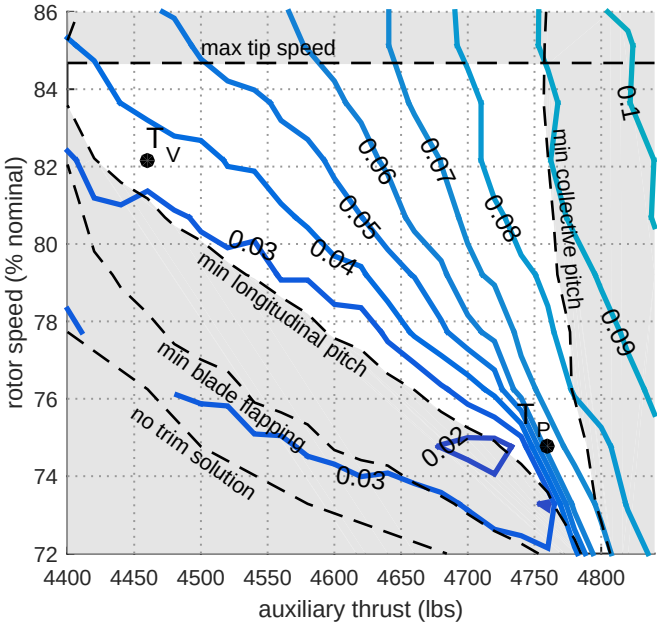

Fig. 4. Map of longitudinal 4/rev hub vibrations (g) for the twisted blade

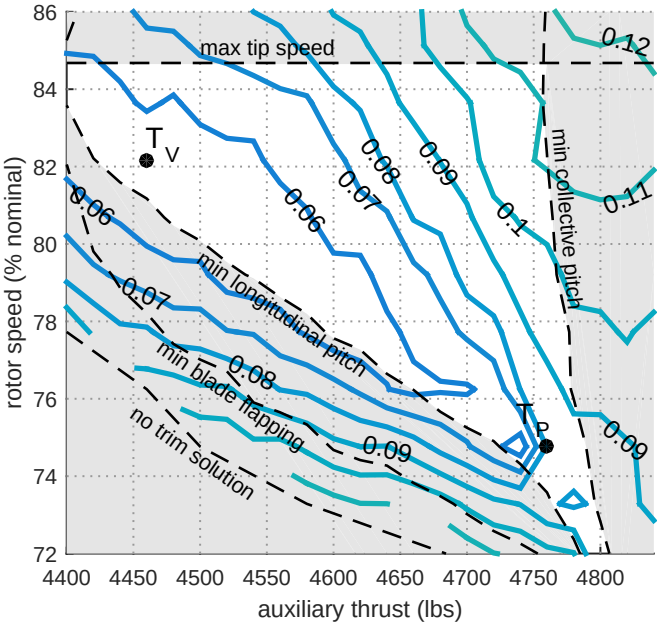

Fig. 6. Map of vertical 4/rev hub vibrations (g) for the twisted blade

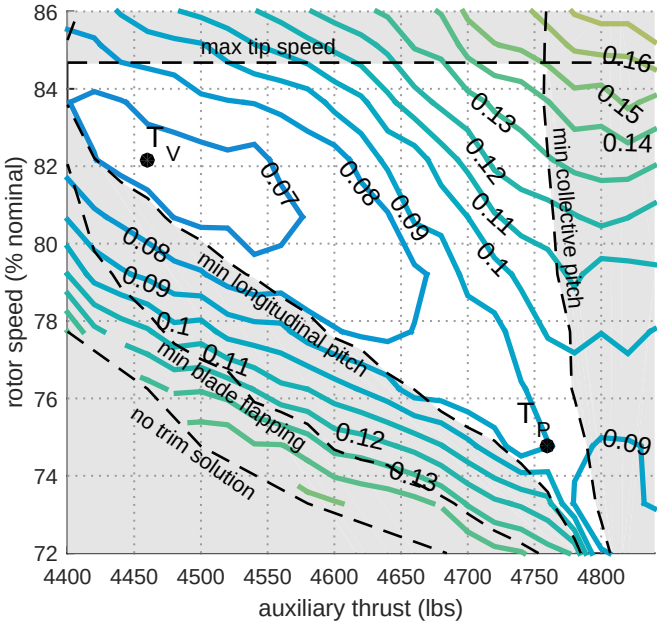

Fig. 5. Map of lateral 4/rev hub vibrations (g) for the twisted blade

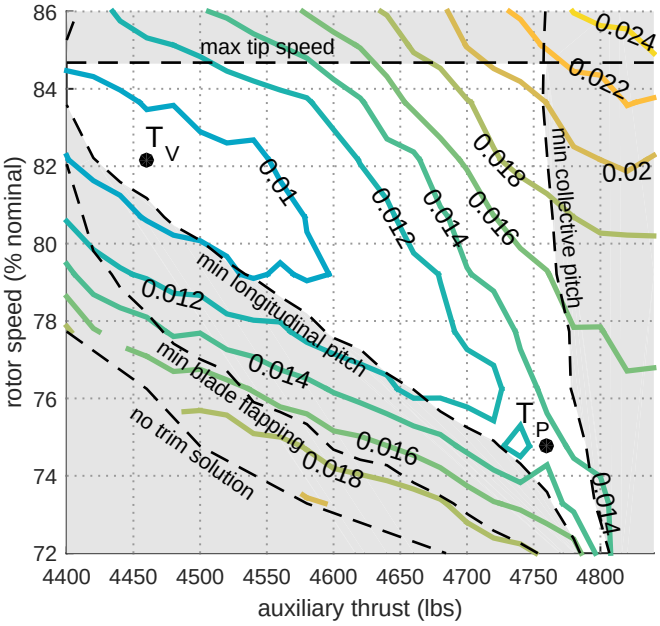

Fig. 7. Map of total 4/rev vibratory hub moments (rad/s^2) for the twisted blade

Table 3. Details of specified trim points

Trim State	T_P	T_V	U_P	U_V
Total Power (hp)	4298	4415	4025	4121
Main Rotor Power	402	801	186	282
Propulsor Power	3896	3614	3839	3839
Rotor Lift Share	16.1%	24.4%	10.5%	11.9%
Wing Lift Share	80.3%	74.1%	84.5%	83.4%
Rotor L/D_e	3.0	3.1	4.0	3.4
Avg. Inflow Ratio	0.051	0.074	0.010	0.016
Additional Controls				
Aux. Thrust (lbs)	4760	4460	4700	4700
Rotor RPM	193	212	181	197
Main Rotor Controls				
Coll. Pitch (θ_{75})	1.7°	6.3°	0.5°	2.1°
Long. Cyclic	−9.6°	−15.6°	1.0°	−1.0°
Lateral Cyclic	−1.1°	0.3°	0.03°	−0.04°
Vehicle Attitude				
Pitch (nose up)	0.54°	0.05°	0.86°	0.78°
Roll (left wing up)	−0.9°	−1.5°	−0.5°	−0.7°
Blade Flap Response				
Coning	0.4°	0.8°	0.3°	0.4°
Long. Flapping	3.3°	6.3°	−0.4°	0.3°
Lateral Flapping	−0.3°	0.3°	0.2°	0.3°
Main Rotor Forces (lbs)				
Thrust (TPP)	3203	4837	2122	2393
H-Force (TPP)	675	972	249	315
Lift (wind)	3237	4914	2121	2395
Drag (wind)	489	435	262	302
Propulsive Thrust	185	531	−13	13
Reverse Flow Region Attributes				
Advance Ratio	0.70	0.64	0.75	0.69
R. F. Power (hp)	−90	−183	−23.8	−12.5
4/rev Hub Force-Vibrations (g)				
Total Vibr.	0.1359	0.0924	0.0388	0.0318
Long. Vibr.	0.0651	0.0355	0.0264	0.0247
Lateral Vibr.	0.0893	0.0658	0.0255	0.0095
Vertical Vibr.	0.0791	0.0544	0.0126	0.0176
4/rev Hub Moment-Vibrations (rad/s^2)				
Total Vibr.	0.0134	0.0092	0.0051	0.0024
Roll Vibr.	0.0037	0.0032	0.0017	0.0005
Pitch Vibr.	0.0053	0.0033	0.0009	0.0014
Yaw Vibr.	0.0118	0.0080	0.0047	0.0019

the UH-60A. Longitudinal cyclic pitch for T_V is −15.6°, which is very close to the minimum bound, and contributes to the large longitudinal flapping angle of 6.3°. As show in Figure 1, the 4837 lbs of thrust and 972 lbs of H-force produced by the rotor in the tip path plane can be resolved in the wind frame to find the total rotor lift and drag. The forward tilt of the rotor positions a component of the thrust to act as propulsive force, in opposition to the rotor drag. Resolving the blade flapping and vehicle attitude angles gives 4914 lbs of rotor lift and 435 lbs of total rotor drag—which includes a 531 lbs reduction in rotor drag due to the propulsive thrust component. As was observed from Figure 2, the rotor of trim state T_V is flapping to provide a component of propulsive thrust to reduce its own drag and account for the low auxiliary thrust. By increasing the auxiliary thrust by 7% (to 4760 lbs), and reducing the rotor speed by 9% (to 193 RPM), the longitudinal cyclic pitch reduces by from −15.6° to −9.6°). Figure 8 shows the difference in azimuthal tip flap response, indicating that the rotor disk at T_P is tilted forward by about half as much as T_V, from 6.3° to 3.3°.

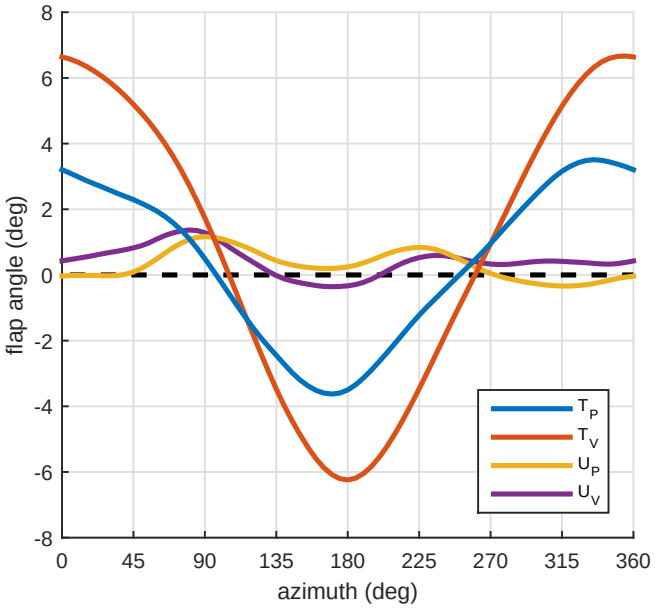

Fig. 8. Blade tip flap response for each trim state

Figure 9 illustrates the difference in sectional S_x about the rotor disk between the two trim states as resolved in the tip path plane. The dotted line on the left hand sides indicate the representative region of reverse flow based on advance ratio, and the boundaries between positive and negative S_x values are indicated by the solid black boundary line. Azimuthal increments of 45° are marked, and the blade is partitioned into four segments by concentric grid lines at 25%, 50%, and 75% span. T_V has a rotor speed of 212 RPM, resulting in a sectional drag force on the advancing tip in excess of 140 lbs/ft. T_P operates at 7% lower RPM (with respect to the nominal speed), and with lower longitudinal pitch angles, resulting in a reduced advancing tip S_x of less than 120 lbs/ft. Despite having a higher advance ratio, T_P also sustains smaller drag forces in the reverse flow region. The dynamic pressures may be larger, but the pitch angles are closer to zero, decreasing the peak magnitude of negative sectional S_x from −140 lbs/ft to −80 lbs/ft. While the negative S_x in the reverse flow region provides torque in the direction of rotation, the low radii at which the forces are applied prevent them from being particularly effective in reducing the rotor power requirement. The S_x on the advancing tip, however, is where the majority of the main rotor power requirement comes from. The radially weighted sectional power plots in Figure 10 illustrate this skew of power contribution towards the more outboard radial stations. In this plot, the value of S_x is multiplied by its dis-

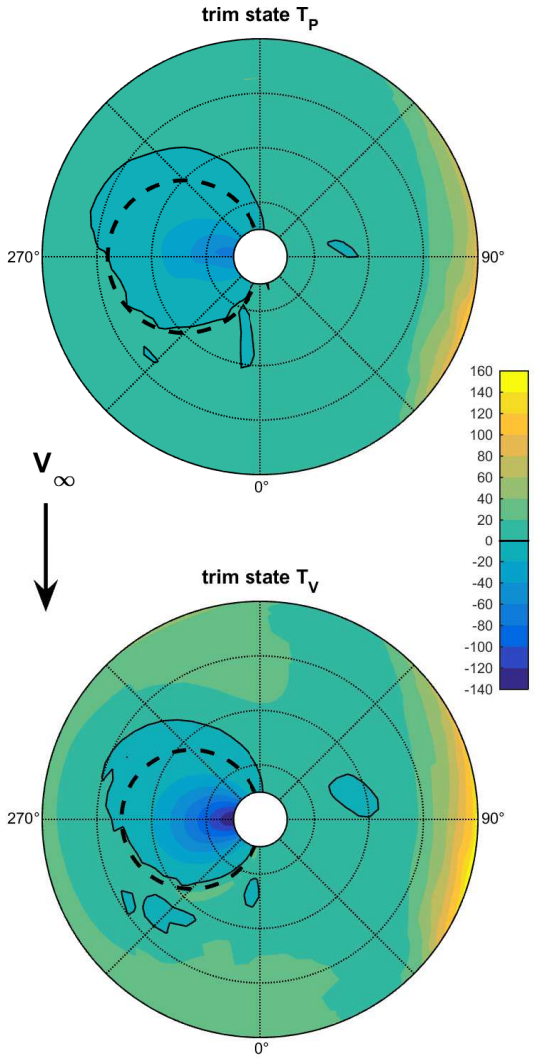

Fig. 9. Rotor disk plots of the sectional blade drag, S_x, (lbs/ft) for the twisted blade

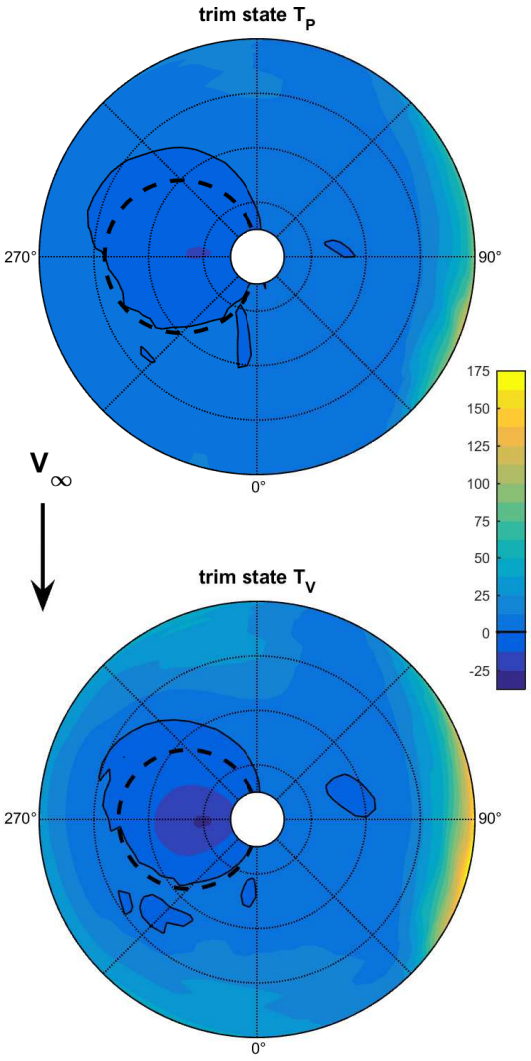

Fig. 10. Rotor disk plots of the distributed power (hp/ft) for the twisted blade

tance from the center of rotation and by the rotational velocity to show which regions have a greater impact in the integrated power. The total main rotor power is therefore the integration of these differential power values. In the case of integrated main rotor power, the drag in the reverse flow region provides assistive torque, which reduces the main rotor power. At trim state T_V, the reverse flow assistive power contribution is -183 hp. For the lower values of reverse flow blade drag at T_P, the power reduction is only -90 hp, which is half as much, but still results in a lower total rotor power due to smaller contributions from the advancing side. As can be expected, the power required to overcome advancing tip drag far exceeds the assistive torque in the reverse flow region, contributing to a total rotor power of 801 hp for T_V, which is nearly twice that of the 402 hp for the low power trim state, T_P.

Figure 11 shows rotor disk plots of sectional S_z about the rotor disk. In both cases there is a large area of negative lift production in the outboard section of the advancing side of the rotor disks. The total area of negative lift is comparable for both cases, but the magnitudes of the negative S_z are 100 lbs/ft larger for trim state T_V. The high lift production at the front and rear of the rotor help it to overcome this negative lift produced at the tip of the advancing blade for a net production of 4914 lbs of lift. Trim state T_P, by comparison produces only -200 to -250 lbs/ft of S_z at the tip—a behavior that can be attributed to having less negative longitudinal pitch and a reduction in rotor speed. A side effect of large thrust production for trim state T_V—which the main rotor uses to overcome the low auxiliary thrust—is that the rotor produces 52% more lift than the 3237 lbs produced by the main rotor at trim state T_P. Of the 20,110 lbs of gross weight, the main rotor at trim state T_V generates 24.4% of the total vehicle lift, and the more efficent wings are left to only generate 74.1%.

In contrast, the increased auxiliary thrust at trim state T_P can accommodate a larger drag force from the main rotor. The reduced rotor speed and longitudinal pitch generates 33% less total thrust and 31% less rotor H-force in the tip path plane as compared to T_V. These forces resolved in the wind frame give

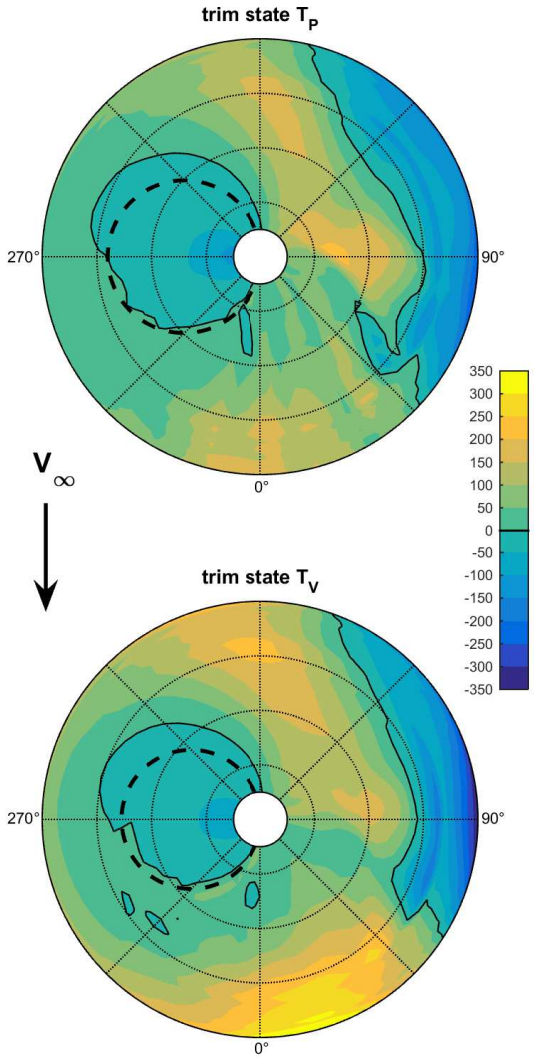

Fig. 11. Rotor disk plots of the sectional blade lift, S_z, (lbs/ft) for the twisted blade

a rotor lift and drag of 3237 and 489 lbs, respectively. Relative to the 531 lbs of propulsive thrust at trim state T_V, the main rotor of trim state T_P flaps much less, and produces only 185 of propulsive thrust in opposition to the rotor drag. While this results in an increase of 65 lbs in the rotor drag force, the 200 lbs increase in auxiliary thrust can more than compensate for it. Rotor lift at trim state T_P is reduced by 1677 lbs, for a rotor lift share of only 16.1%. With the rotor producing less lift, the vehicle pitches nose-up by an additional 0.5°, and increases the wing lift share from 74.1% to 80.3%. With a larger fraction of the lift transferred to the more efficient lifting system, trim point T_P accomplishes a 399 hp reduction in main rotor power with only an additional 200 lbs of thrust and 282 hp required from the propulsor. In summation, trim state T_P improves upon the performance of the vehicle at trim state T_V by 3%—relaxing the power requirements from 4415 hp to 4298 hp.

Trim for Low Vibrations

In exchange for the 3% increase in power requirements, trimming at T_V provides a 32% reduction in 4/rev total force vibration magnitude as compared to trim state T_P. For trim state T_P, the vehicle pitch is 0.54° nose up, the longitudinal flapping is 3.3°, and the rotor thrust is 3203 lbs, for a coefficient of thrust of 0.0022, and a mean inflow ratio of 0.051. For such a low lifting rotor at such high speeds, the vortices shed at the rotor tip and between the negative and positive lift regions on the advancing blade will primarily advect with the free stream velocity, as the induced strength of an unloaded rotor is very small. Figure 12 shows the difference in the wake angles between the two cases, with 20× magnification in the vertical distance to highlight the differences. For trim state T_V, the increased inflow ratio (0.074) carries the shed vortices with a greater vertical component, which will decrease the impulsive changes observed at the rotor disk. In addition, the increased flapping of the low vibration state is also visible at this scale.

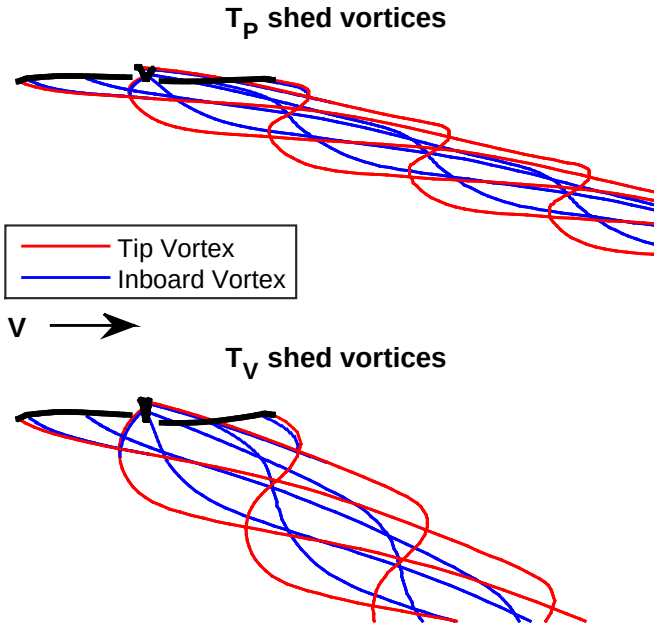

Fig. 12. Shed vortices of the twisted blade states, with 20× magnification in vertical direction

The effects that the behavior of the shed vortices incurs on the induced velocity of the rotor disk can be observed from Figure 13. The combination of a nearly horizontal rotor wake, a nose-up vehicle pitch, and small longitudinal blade flapping results in the shed vortices of the advancing and retreating blades being the dominant contributor to the induced velocity at the rear of the rotor disk. Figure 13 shows the induced velocity distribution over the rotor disk, with positive values for rotor downwash and negative values for rotor upwash. For both rotor disks, the inflow on the front half of the rotor disk ranges from −10 to 15 ft/s, but when the blades are in the path of the shed vortices at the rear of the disk, the induced velocities of trim state T_P range from −30 to 40 ft/s. At the

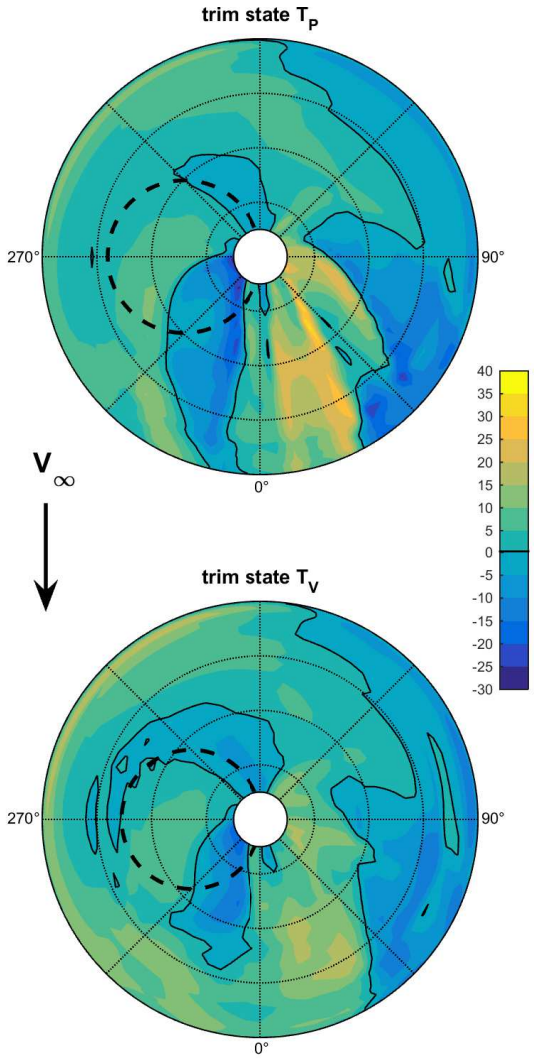

Fig. 13. Rotor disk plots of the induced velocity (ft/s) for the twisted blade

low vibration trim state, T_V, the 0.05° nose-up pitch is more level, and the longitudinal flapping is 6.3°. These factors contribute to raising the blade out of the path of the shed vortices for a narrower range of induced velocities between −20 and 20 ft/s at the rear of the disk. With both sets of induced velocity plotted on the same scale, Figure 13 demonstrates that the increased flapping of trim state T_V reduces the impulsive influence of the shed vortices on the induced velocity at the rear of the rotor disk.

The bands of induced velocity fluctuation at the rear of the disk cause changes in the angle of attack at the blade, which in turn translate into higher harmonic fluctuations in the aerodynamic forces at the blade. For trim state T_P, evidence of higher harmonic aerodynamic fluctuations can be seen in examination of the contours at the rear of the disk in Figure 11. Even with the low contour density in this region, there is a definitive presence of peaks and valleys in the sectional S_z plot for trim state T_P. This can be best observed at 75–80% span between the 330° and 60° azimuth angles. As the blade progresses at the rear of the disk, it encounters relative peaks in sectional S_z at 345°, 35°, and 55°, corresponding to high rotor up-wash in Figure 13. There are also valleys at 10°, 30°, and 50°, which correspond to larger values of rotor down-wash. Ignoring peaks in sectional S_z that can be attributed to blade flapping, the only observable fluctuation in the disk plot for trim state T_V occurs at 55°. This is also the azimuthal location of the only peak in rotor down-wash for T_V in Figure 13.

Figure 14 provides the shear forces normal to the blade at 20%, 50%, and 70% span for both T_P and T_V as a function of azimuth, with gray shading to represent the reversed flow region. At all three radial stations, the magnitudes of the higher harmonic content appears larger for trim state T_P. Transforming the shear loads from the time-domain into the frequency-domain gives a 4/rev amplitude for the normal shear loading which confirms this observation. These values are reported at four different radial spans in Table 4. For each of the radial stations, the 4/rev normal shear forces are larger in magnitude for trim state T_P. In the vertical direction, the rotor hub filters out all vibratory loads that are transferred at the blade root except for the 4/rev vertical shear forces, for which the primary contributor is the shear force normal to the blade. The 31% reduction in vertical hub vibrations—from 0.0791g to 0.0544g—that is achieved at trim state T_V can therefore be correlated to the 47% reduction in normal blade shear forces at the root. With similar reductions occurring across all internal loads and moments, the 32% reduction of total 4/rev hub force vibration and the 31% reduction of total 4/rev hub moment vibrations can be attributed to the position of the blades at the rear of the disk, as increased longitudinal flapping moves the blade path out of the path of the shed vortices in the wake of the preceding blades.

Table 4. 4/rev normal shear force magnitude (lbs)

Radial Position	T_P	T_V	U_P	U_V
Root	39.6	21.0	10.4	11.0
20% R	3.1	2.0	1.8	2.6
50% R	24.8	18.1	3.2	7.7
70% R	7.0	6.4	1.5	5.3

UNTWISTED BLADE RESULTS

Reducing the twist rate of a blade generally results in an improvement to rotor performance in high speeds (Refs. 17, 21). To examine the potential to improve rotor performance and reduce vibration levels of untwisted blades by exploiting control redundancy, parametric variations in auxiliary thrust and rotor speed are repeated for an untwisted rotor. Figure 15 shows contours of total power requirements over a range of rotor speed and auxiliary thrust variation. While the range for auxiliary thrust is still 4400–4860 lbs, the minimum longitudinal pitch and blade flapping constraints that were present for the twisted rotor (at the bottom left in Figures 2–7) have receded, opening up a larger feasible region for more reduction in RPM. The total power contours exhibit similar behavior to

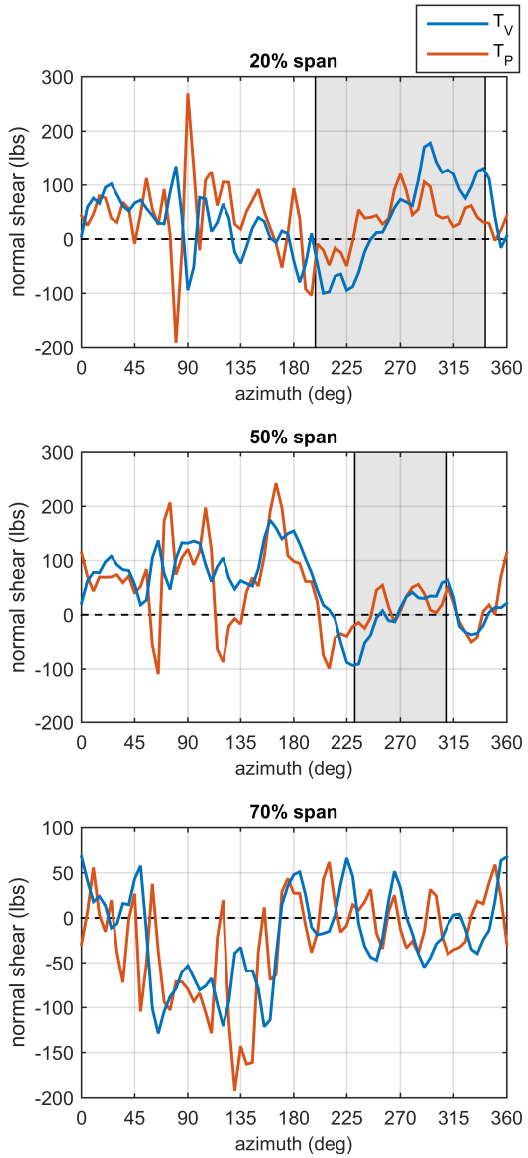

Fig. 14. Normal shear (lbs) for the twisted rotor (positive up)

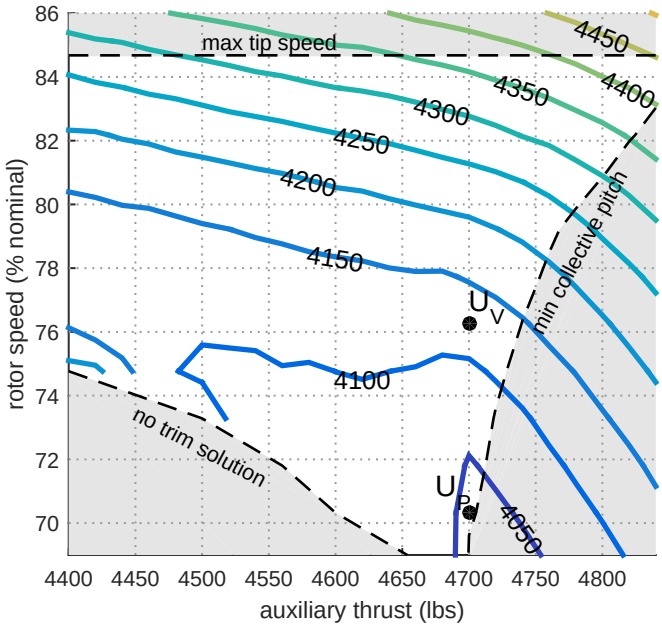

Fig. 15. Map of total power (hp) for the untwisted blade

that of the twisted rotor in Figure 2, but for any combination of auxiliary thrust and rotor speed, the untwisted rotor has a lower total power than the corresponding case for the twisted rotor. When the rotor is untwisted, the bound on collective pitch—which was defined with respect to the 75^{th} spanwise station—does not change. The main rotor hub could be designed to allow lower collective pitches, but since it is not significantly impinging on the minimum power point, the lower bound is left as is. Trim states U_P and U_V are selected at low power and low vibration points, respectively, and tabulated for comparison alongside trim states U_P and U_V in Table 3.

Trim for Low Power

The lowest untwisted rotor powers occur when the rotor RPM is close to the minimum, as constrained by the boundaries of minimum collective pitch and absence of converged trim solutions. A low power trim state close to the minimum collective pitch boundary is selected and labeled U_P. In comparison to the low power point of the twisted rotor, T_P, trim state U_P operates with 60 lbs (1.3%) less auxiliary thrust, and at a rotor speed a rotor speed that is reduced by an additional 5% of the nominal rotor speed. The total power requirements are reduced by 6.4%, from 4298 hp to 4025 hp. Of this reduction, only 63 hp comes from the reduction in auxiliary thrust, while the remaining 216 hp comes from reduction in main rotor power, a reduction of 54%.

The reduction in main rotor power is due to a fundamental difference in the operation of the untwisted blade. Figure 16 shows the blade sectional drag in the hub plane for the untwisted rotor. Relative to the sectional S_x force of the twisted rotor at low power, the drag levels of the untwisted rotor at low power are greatly reduced. Relative to Figure 9, the contour scaling has been reduced by half. At the tip, the sectional S_x has been reduced from about 120 lbs/ft to about 70 lbs/ft. Within the reverse flow region, the benefit is even greater, where the peak drag is reduced from -80 lbs/ft to -5 lbs/ft. Even with a larger reverse flow region (resulting from the reduced rotor speeds), the 94% reduction in peak reverse flow drag helps produce an 86% reduction in integrated reverse flow drag, which in turn contributes to a 46% reduction in total rotor drag. While the longitudinal pitch in the reverse flow region may be as important for rotor drag reduction as the advancing tip pitch, it has a smaller effect on the total rotor power, which is shown in Figure 17. With the reduced main rotor drag, there is only -24 hp of assistive power in the reverse flow region, thus the reduced advancing tip drag is the main cause of the 54% reduction in main rotor power.

The conventional main rotor controls for the twisted blade trim state, T_P, are trimmed with a collective pitch of 1.7° and a longitudinal pitch of -9.6°. On the advancing blade, where

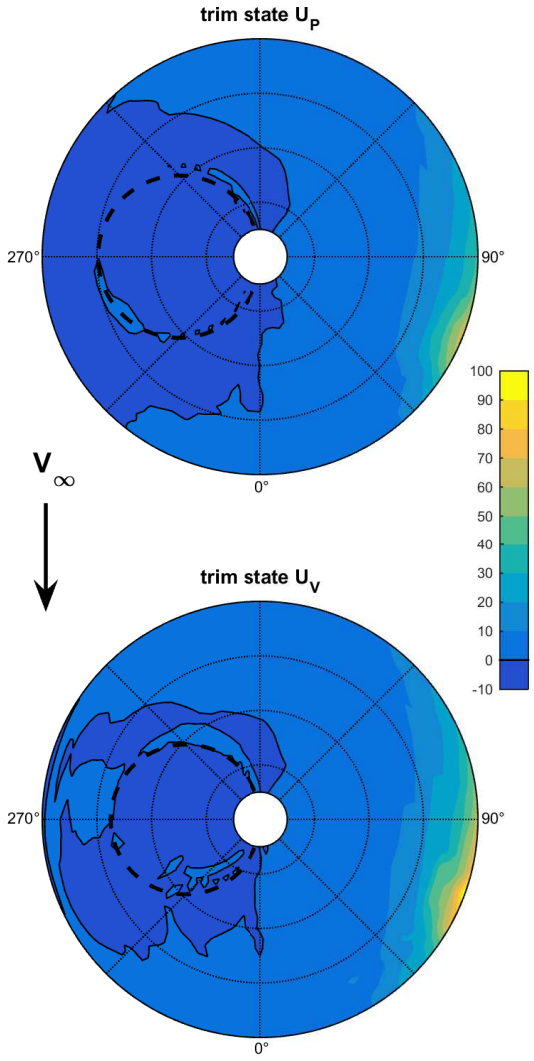

Fig. 16. Sectional blade drag (*Sx*) rotor disk plots for the untwisted blade

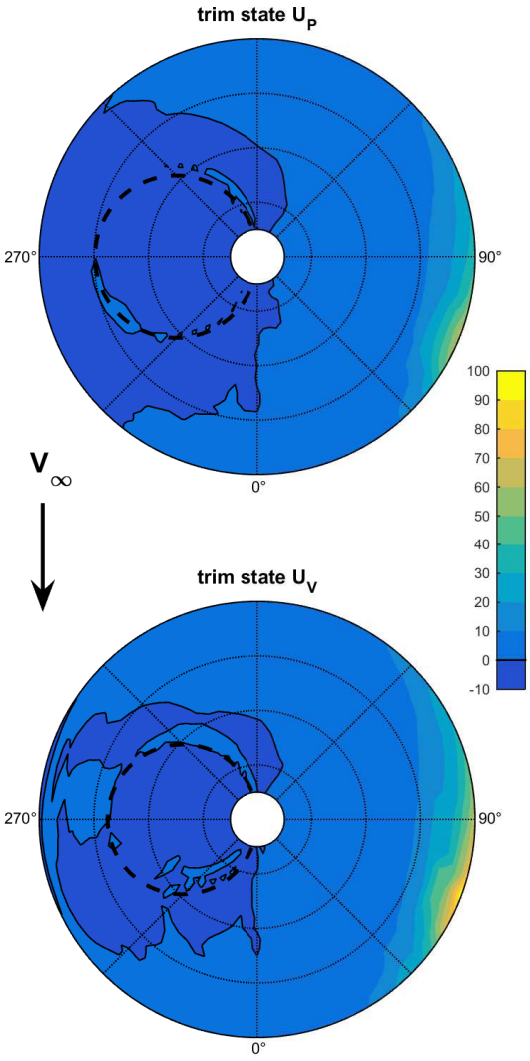

Fig. 17. Distributed power rotor disk plots for the untwisted blade

dynamic pressures are the highest, this pitch input results in $-7.9°$ at the 75^{th} spanwise station, and a tip pitch of $-9.9°$. For the untwisted rotor at trim state U_P, the $0.5°$ of collective and $1.0°$ of longitudinal put the entire undeformed blade at a pitch of $1.5°$ for the $90°$ azimuth. These two states are compared side by side in Figure 18. The decrease in main rotor power is attributed to the reduction in blade pitch on the advancing tip, and to the reduction in dynamic pressure associated with reducing the rotor speed.

In trim state T_P, the large negative values of longitudinal pitch produce large longitudinal flapping angles, but for trim state U_P, blade flapping is greatly reduced, as can be seen from the values in Table 3. Figure 8 includes the blade tip flap response of the untwisted rotor trim states for comparison with the twisted rotor flapping. The large flapping angles in the case of the twisted rotor tilt the tip path plane forward, and orient a component of rotor thrust in the longitudinal direction such that the total rotor drag is reduced. In producing negative lift on the advancing tip to flap the blade, the twisted rotor produces enough positive thrust elsewhere on the rotor disk to offset the negative lift and a portion of the rotor drag. The positive thrust vector of 3203 lbs with $3.8°$ of forward tilt adds a propulsive component of 185 lbs, for a total rotor drag of 489 lbs, which can successfully equilibrate with the remaining body forces acting on the aircraft. All of the excess lift generated to oppose the rotor drag is accompanied by high profile and induced drag, which affects not only the total rotor drag, but the rotor power. Simply stated, to reduce its own drag, the rotor is producing excessive, opposing aerodynamic forces which successfully cancel each other out, but with 402 hp of rotor power.

In contrast to the twisted rotor, the uniform geometry of the untwisted blade allows it to reduce its drag by reducing the profile along the span. Figure 18 demonstrates that for any pitch angle the twisted blade is set, there are large angles of attack at least somewhere along the span, but with the untwisted blade a pitch can be specified such that the entire blade has a minimal frontal area, reducing profile drag. Rather than tilt-

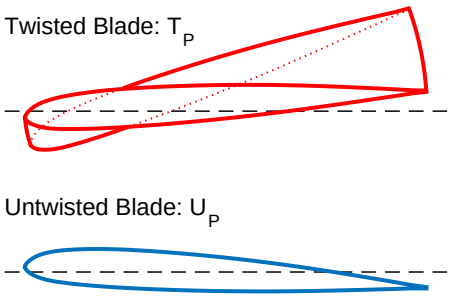

Fig. 18. Blade twist and pitch comparison at 90° azimuth, viewed from root to tip, with 2× magnification of angles

ing the tip path plane to produce propulsive thrust, trim state U_P has 0.4° of rotor blowback, generating 2121 lbs of lift and 262 lbs of rotor drag. In Figure 19, trim state U_P is producing lower magnitudes of negative S_z over a smaller region of the advancing tip, and less positive S_z over the rest of the rotor disk when compared to trim state T_P in Figure 11. Producing less lift also reduces the drag production. By not generating excess internal aerodynamic forces in the rotor system, both the total rotor drag and the rotor power (186 hp) are reduced from that of the twisted rotor. In addition, the lower rotor drag allows a gain in performance accompanying the lower auxiliary thrust necessary to trim the aircraft. In addition, the lift of the main rotor is reduced from 3237 lbs to 2121 lbs, which results in the wings producing a greater fraction of the vehicle lift with better efficiency.

Untwisting the rotor to achieve high speed rotor performance comes as a trade-off for a reduction in hover performance. As the blade twist moves further from ideal twist, the hover power will increase. The hover performance penalties are calculated using a 12×12 state dynamic inflow in hover for both rotor twists at 258 RPM, and with no auxiliary thrust. From Table 5, the twisted rotor hovers with a power of 2156 hp and the untwisted rotor hovers with 2286 hp. Based on the mission for which a compound helicopter is designed, the 273 hp reduction in high speeds may or may not be worth the additional 130 hp in hover.

Table 5. Comparison of hover performance

Blade	Twisted	Untwisted
Hover Power (hp)	2156	2286
Main Rotor Controls		
Coll. Pitch (θ_{75})	7.3	7.6
Long. Cyclic	−2.6	−2.3
Lateral Cyclic	1.8	2.0
Vehicle Attitude		
Pitch (nose up)	2.3	2.1
Roll (left wing up)	−2.2	−2.4
Blade Flap Response		
Coning	3.7	4.0
Long. Flapping	2.3	2.1
Lateral Flapping	2.3	2.1

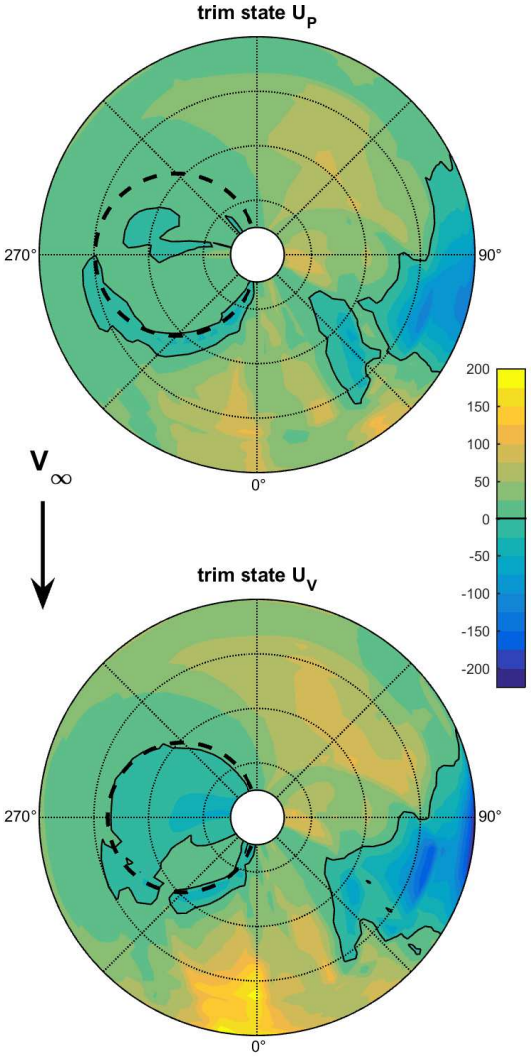

Fig. 19. Sectional blade lift (S_z) rotor disk plots for untwisted blade

In summary, the untwisting of the rotor blade in conjunction with appropriate settings for additional controls at 225 kts results in a 54% reduction in main rotor power, and a 6.4% reduction in total power as compared to the twisted rotor at a cost of 6.0% more power required to hover.

Trim for Low Vibrations

In Figure 20, the minimum of the total 4/rev hub vibratory force occupies a region close to the low power case, U_P. Figures 21, 22, and 23 give the longitudinal, lateral, and vertical components of vibratory hub forces expressed in g. The total 4/rev vibratory hub moment is mapped in Figure 24, which follows trends similar to the total 4/rev vibratory hub force. Relative to trim state T_V, trim state U_P has not been minimized for vibrations, but still sees a 58% reduction in total vibratory hub forces (reduced by 0.0536g). The longitudinal vibrations are reduced by 26% (0.0091g), but the majority of the reduction comes from the 61% reduction in lateral vibrations (0.0403g) and the 77% in vertical vibrations (0.0418g).

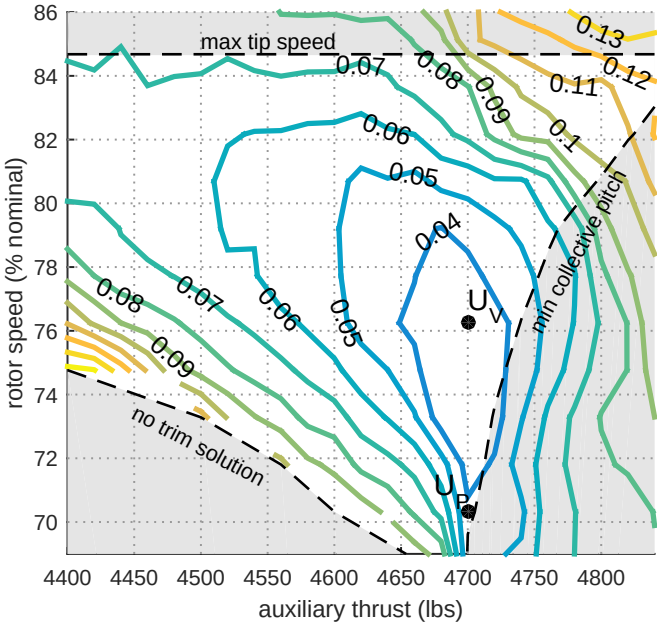

Fig. 20. Map of total 4/rev vibratory hub forces (g) for the untwisted blade

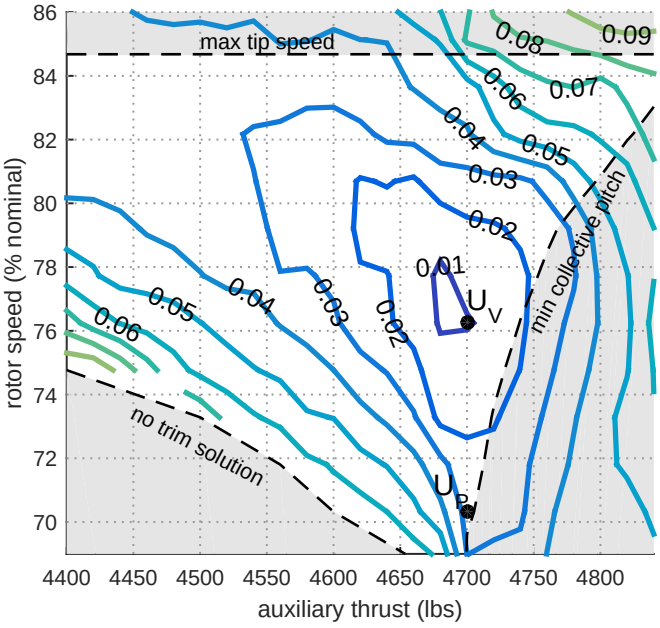

Fig. 22. Map of lateral 4/rev hub vibrations (g) for the untwisted blade

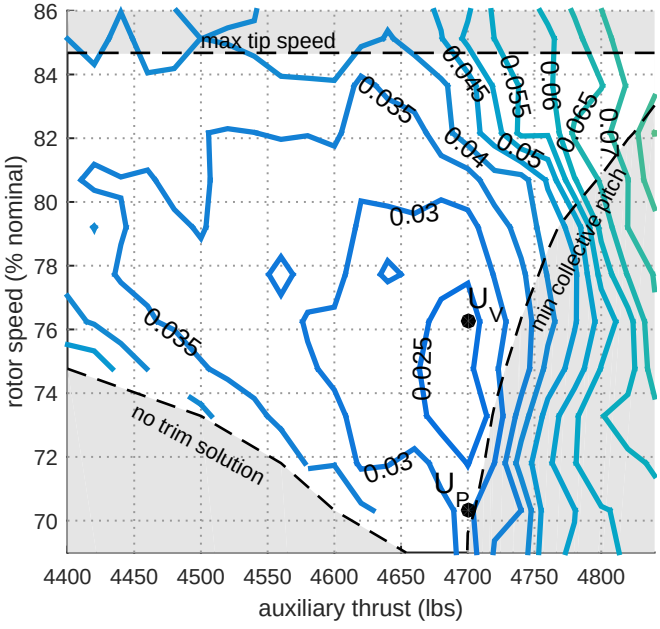

Fig. 21. Map of longitudinal 4/rev hub vibrations (g) for the untwisted blade

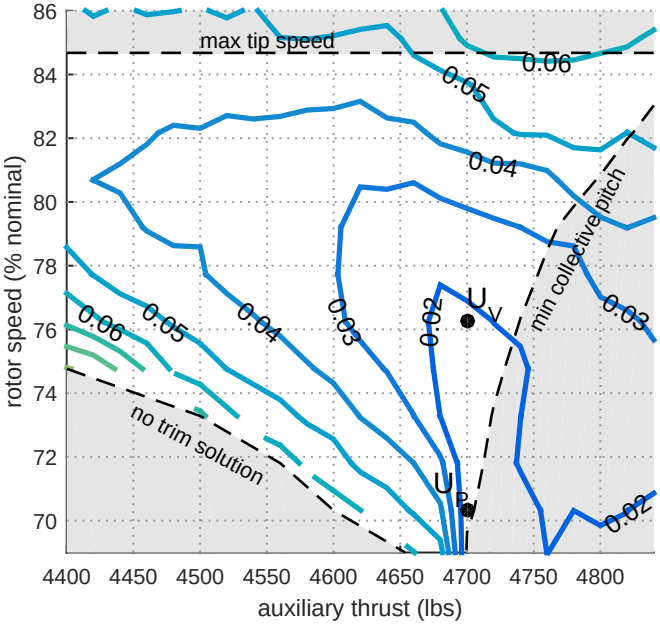

Fig. 23. Map of vertical 4/rev hub vibrations (g) for the untwisted blade

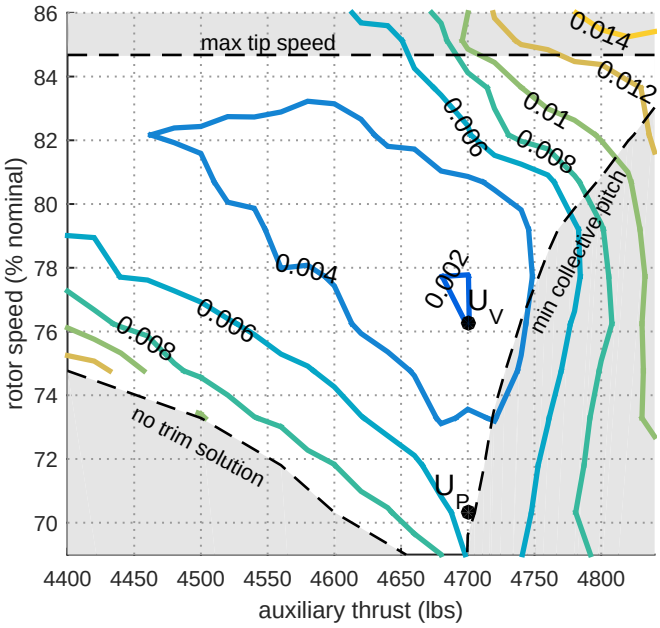

Fig. 24. Map of total 4/rev vibratory hub moments (rad/s^2) for the untwisted blade

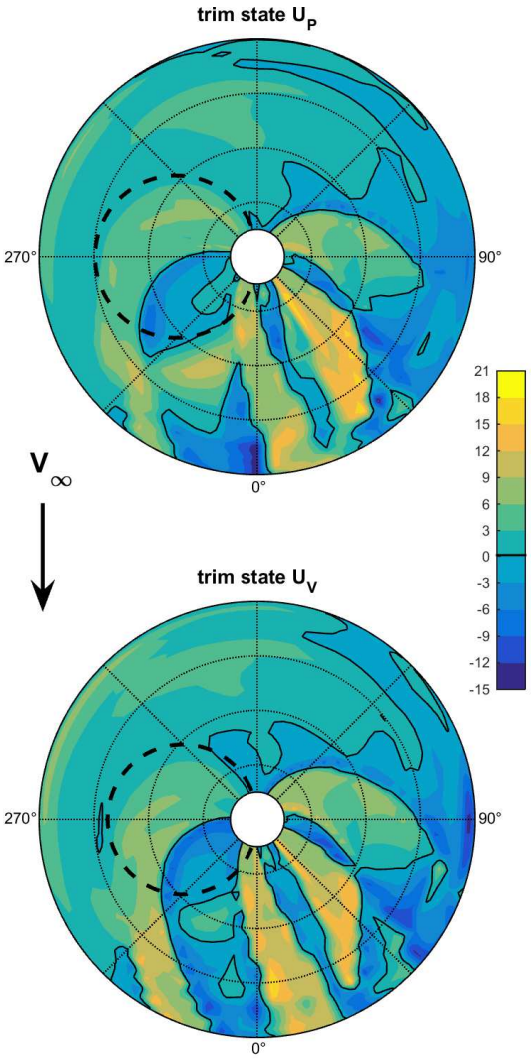

Fig. 25. Induced velocity rotor disk plots for the untwisted blade

For an untwisted rotor that is trimmed for low vibrations (U_V), the vibrations are 66% lower than they were at trim state T_V. Comparing U_V to U_P, the longitudinal vibration component remains about the same, but U_V exchanges a 40% increase in vertical vibrations for a 63% reduction in lateral vibrations. The total 4/rev vibratory forces are thus reduced by 18%, from 0.0388g to 0.0318g.

The low vibrations relative to the twisted rotor can be attributed to the reduced magnitude of the impulses in the induced velocity. Although some impulsive changes in inflow are observed in Figure 25, the range of variation is smaller than was observed in Figure 13 for the twisted rotor (which used a larger scale), despite the significantly lower longitudinal blade flapping angles. The reduction in total rotor thrust from 4837 lbs at trim state T_V to 2393 lbs at trim state U_V contributes to a reduction in the mean inflow ratio of 86%. This in turn reduces the strength of the shed vortices and their effect on the induced velocity—such that even without the large longitudinal flapping to position the blade above the shed vortices, the magnitude of the positive and negative impulses in the inflow are smaller than they were for trim state T_V in Figure 13, In contrast to the twisted rotor trim states, both trim states U_P and U_V are subject to the same range of induced velocities, demonstrating that there is no significant change in the rotor mechanics between the two states.

In Figure 20, trim state U_P is located within a narrow band of low vibrations, between an infeasible region at higher rotor thrust, and steep contours of increased vibratory forces for lower auxiliary thrusts. It can be inferred that the auxiliary thrust provided at trim state U_P is ideal, such that it is unnecessary for the main rotor to provide any additional propulsive thrust to satisfy vehicle equilibrium. Moving to lower auxiliary thrusts along constant rotor speed, the trim states experience a sharp increase in vibratory force magnitudes. At such low rotor speeds, trim state U_P takes advantage of a finely tuned balance of rotor drag and propulsor thrust to minimize vibrations and power by trimming with near-zero pitch controls, but the vibration levels double with only a 50 lbs reduction in auxiliary thrust. The low rotor speed increases the advance ratio to 0.75, which reduces the authority of the longitudinal pitch control. Producing this propulsive thrust despite the poor control authority results in large increases in vibrations, so trim point U_P can be considered close to the lower desirable limit of rotor speed reduction. The low vibration region at higher rotor speeds, in which U_V resides, can handle greater variations in auxiliary thrust without incurring large increases in vibration. In this sense, trim state U_V is at a more robust state of low vibration.

For an increase in rotor speed 6% with respect to the nominal RPM, the main rotor power increases from 186 hp to

282 hp, and the total 4/rev hub force vibrations decrease from 0.0388g to 0.0318g—an 18% improvement in vibrations for a 2.3% penalty to total vehicle power. The 0.007g of vibration reduction may only be an 18% improvement compared to trim state U_P, but when compared against the 77% reduction from the 0.1359g total 4/rev hub vibrations of trim state T_P, it is a less significant reduction. Neither the 0.007g difference in vibration nor the 104 hp difference in main rotor power demonstrate a fundamental change in rotor operation between the two untwisted states. A compound helicopter at 225 kts with a twisted blade has the option of exploiting control redundancies to minimize either power or vibrations, but for a rotor with an untwisted blade, this result suggests that minimization of either power or vibration results in a near minimal state for both optimization criteria.

CONCLUSIONS

The present study examines trim of an articulated compound helicopter, invoking redundant controls as a tool for minimization of rotor power and hub vibrations in high speed flight at 225 kts. It compares the fundamental characteristics of a lightly loaded main rotor with both twisted and untwisted blades at near-optimal control settings and draws the following conclusions. Simulations were based in RCAS using a model derived from the UH-60A, with 20,110 lbs gross weight, reduced flat plate drag area, reduced blade twist, a lifting wing, and an auxiliary propulsor.

For -8° linearly twisted blades, minimization of power is accomplished at an optimal combination of main rotor power and propulsor power. The main rotor is trimmed at 75% nominal rotor speed with a small positive value of longitudinal flapping. This reduces rotor drag, auxiliary thrust, and corresponding propulsor power without overly increasing the rotor power through excessive profile and induced drag on the advancing tip. For a low power case study which obeyed the control limits, the longitudinal flapping was only 3.3°, and the wing lift share was 80.3%. The rotor power was 402 hp, for a total vehicle power of 4298 hp.

To minimize the vibrations at the hub, the auxiliary thrust is lowered by 6%, and the rotor speed is increased to 82% of nominal speed. In the new trim state, the rotor must accommodate for the lower auxiliary thrust by reducing its drag. This is done by producing additional rotor thrust and tilting the tip path plane further forward. The longitudinal flapping increases to 6.3°, and with the addition of more rotor thrust, the wing lift share reduces to 74.1%. The increased thrust from the rotor and larger forward flapping angles contribute to raising the blades at the rear of the disk out of the path of the vortices shed from the preceding blades on the advancing side. The reduction in impulsive induced velocity reduces the higher harmonic content in the aerodynamic forces, which in turn reduces the total vibrations at the hub. By trimming to reduce vibrations, the total 4/rev hub force vibrations of the case study are reduced by 32% in exchange for a 3% increase in total power.

Untwisting the blade allows it to achieve a minimum power state where its frontal area on the advancing side can be minimized by reducing the pitch controls to near-zero values. Compared to the low power trim state of the twisted rotor, the production of negative lift on the advancing side of the rotor disk is dramatically reduced in size and in magnitude. The near-zero longitudinal pitch inputs and 5% lower rotor speed allow the blade drag on the advancing tip and in the reverse flow region to reduce significantly, resulting in less main rotor power. In addition, the reduced total rotor drag allows vehicle equilibrium with lower auxiliary thrust, and therefore lower propulsor power. The overall reduction in vehicle power is 6.3% between the twisted and untwisted low power cases, with most of the difference accounted for in the 54% reduction in rotor power.

Relative to the minimum vibration state of the twisted rotor, the untwisted rotor sees a reduction across all components of vibration, but the greatest reductions occur in the lateral and the vertical directions. Where the minimum vibration and minimum power trim states of the twisted rotor occupy two distinct regimes, there is only a slight difference between the minimum power and minimum vibration states of the untwisted rotor. All states in this regime operate at both better performance and lower vibrations than the minimum states of the twisted rotor. By untwisting the blade, the minimum power trim state of the twisted rotor is improved by 4–6.3% within this optimal region, and the total 4/rev hub vibratory forces are reduced by 57–66% from the lowest vibration trim states for the twisted rotor.

Author contact: Jean-Paul Reddinger, reddij2@rpi.edu; Farhan Gandhi, fgandhi@rpi.edu; Hao Kang, hao.kang2.civ@mail.mil

ACKNOWLEDGMENTS

This research was funded by the U.S. Government under Agreement No. W911W6-11-2-0011. The U.S Government is authorized to reproduce and distribute reprints notwithstanding any copyright notation thereon. The views and conclusions contained in this document are those of the authors and should not be interpreted as representing the official policies, either expressed or implied, of the U.S. Government.

REFERENCES

[1]Leishman, J. G., *The Helicopter—Thinking Forward, Looking Back*, College Park Press, College Park, MD, 2007.

[2]Ruddell, A., "Advancing Blade Concept (ABC) Technology Demonstrator," U. S. Army Research and Technology Labotratories (AVRADCOM), USAAVRADCOM-TR-81-D-5, Apr. 1981.

[3]Bagai, A., "Aerodynamic Design of the X2 Technology^{TM} Demonstrator Main Rotor Blade," American Helicopter Society 64^{th} Annual Forum, Montréal, QC, Canada, Apr. 29–May 1, 2008.

[4]Blackwell, R., and Millott, T., "Dynamics Design Characteristics of the Sikorsky X2 Technology^{TM} Demonstrator Aircraft," American Helicopter Society 64th Annual Forum, Montréal, QC, Canada, Apr. 29–May 1, 2008.

[5]Walsh, D., Weiner, S., Arifian, K., Bagai, A., Lawrence, T., and Blackwell, R., "Development Testing of the X2 Technology^{TM} Demonstrator," American Helicopter Society 65th Annual Forum, Grapevine, TX, May 27–29, 2009.

[6]Walsh, D., Weiner, S., Arifian, K., Lawrence, T., Wilson, M., Millott, T., and Blackwell, R., "High Airspeed Testing of the Sikorsky X2 Technology^{TM} Demonstrator," American Helicopter Society 67th Annual Forum, Virginia Beach, VA, May 3–5 2011.

[7]Colucci, F., "No Single Decision." *Vertiflite*, Nov./Dec. 2014: 10–11.

[8]Hirschberg, M., "Raider Rolls Out." *Vertiflite*, Nov./Dec. 2014: 12–13.

[9]Prouty, R. W., and Yackle, A. R., "The Lockheed AH-56 Cheyenne—Lessons Learned," AIAA-92-4278, AIAA Aircraft Design Systems Meeting, Hilton Head, SC, Aug. 24–26, 1992.

[10]Johnson, W., Yeo, H., and Acree, C. W., "Performance of Advanced Heavy-Lift, High-Speed Rotorcraft Configurations," AHS International Forum on Multidisciplinary Technology, Seoul, Korea, Oct. 15–17, 2007.

[11]Colucci, F., "SpeedHawk—Phase I." *Vertiflite*, Winter 2007.

[12]Nelms, D., "Aviation Week Flies Eurocopters X^3" *Aviation Week & Space Technology*, Vol. 174, No. 24, Jul. 9, 2012.

[13]Balmford, D. E. H., and Benger, B. S., "The Compound Helicopter—A Concept Revisited," 17th European Rotorcraft Forum, Berlin, Germany, Sept. 1991.

[14]Humpherson, D. V., "Compound Interest—A Dividend for the Future, Revised," American Helicopter Society 54th Annual Forum, Washington DC, May 2022, 1998.

[15]Orchard, M. N., and Newman, S. J., "The Compound Helicopter Versus Tilt Rotor—Europes Shortcut to the Future," 26th European Rotorcraft Forum, The Hague, Netherlands, Sept. 2000.

[16]Yeo, H., and Johnson, W. "Optimum Design of a Compound Helicopter," Presented at the Heli Japan 2006 AHS International Meeting on Advanced Rotorcraft Technology and Life Saving Activities, Nagoya, Japan, Nov. 2006.

[17]Yeo, H., and Johnson, W., "Aeromechanics Analysis of a Heavy Lift Slowed-Rotor Compound Helicopter," *Journal of Aircraft,* Vol. 44, (2), Mar./Apr. 2007, pp. 501–508.
doi: 10.2514/1.23905

[18]Floros, M. W., and Johnson, W., "Performance Analysis of the Slowed-Rotor Compound Helicopter Configuration," Vol. 54, (2), Apr. 2009, pp. 1–12.
doi: 10.4050/JAHS.54.022002

[19]Ormiston, R. A., "Low-Disk Loading Compound Rotorcraft for High Speed and Aerodynamic Efficiency," AHS, AIAA, SAE, RAeS International Powered Lift Conference Proceedings, Philadelphia, PA, Oct. 5–7, 2010.

[20]Hall, K. C., and Hall, S. R., "A Variational Method for Computing the Optimal Aerodynamic Performance of Conventional and Compound Helicopters," Vol. 55, (4), Oct. 2010, pp. 1–16.
doi: 10.4050/JAHS.55.042006

[21]Moodie, A. M., and Yeo, H., "Design of a Cruise-Efficient Compound Helicopter," *Journal of the American Helicopter Society,* Vol. 57, (3), Jul. 2012, pp. 1–11.
doi: 10.4050/JAHS.57.032004

[22]Rand, O., and Khromov, V., "Compound Helicopter: Insight and Optimization," *Journal of the American Helicopter Society,* Vol. 60, (1), Jan. 2015, pp. 1–12.
doi: 10.4050/JAHS.60.012001

[23]Datta, A., Yeo, H., and Norman, T. R., "Experimental Investigation and Fundamental Understanding of a Full-Scale Slowed Rotor at High Advance Ratios," *Journal of the American Helicopter Society,* Vol. 58, (2), Apr. 2013, pp. 1–12.
doi: 10.4050/JAHS.58.022004

[24]Sekula, M. K., and Gandhi, F., "Effects of Auxiliary Lift and Propulsion on Helicopter Vibration Reduction and Trim," *Journal of Aircraft,* Vol. 41, (3), May–Jun. 2004, pp. 645–656.

[25]Gandhi, F., and Sekula, M. K., "Helicopter Vibration Reduction using Fixed-System Auxiliary Moments," *AIAA Jounral,* Vol. 42, (3), Mar. 2004, pp. 501–512.

[26]Sekula, M. K., and Gandhi, F., "Helicopter Vibration and Rotor Power Reduction through Horizontal Tail Incidence Angle Control," American Helicopter Society 60th Annual Forum, Baltimore, MD, Jun. 7–10, 2004.

[27]Gandhi, F., and Sekula, M. K., "Helicopter Horizontal Tail Incidence Control to Reduce Rotor Cyclic Pitch and Blade Flapping," American Helicopter Society 60th Annual Forum, Baltimore, MD, Jun. 7–10, 2004.

[28]Barron, H. M., Brentner, K, Horn, J. F., Ozdemir, G. T., and Thorsen, A. T., "Acoustic Analysis of Compound Helicopters with Trim Variations," American Helicopter Society 69th Annual Forum, Phoenix, AZ, May 21–23, 2013.

[29]Thorsen, A., Horn, J. F., and Ozdemir, G. T., "Use of Redundant Controls to Enhance Transient Response and Handling Qualities of a Compound Rotorcraft," American Helicopter Society 70th Annual Forum, Montréal, QC, Canada, May 21–23, 2014.

[30]Ozdemir, G. T., Horn, J. F., and Thorsen, A., "In-Flight Multi-Variable Optimization of Redundant Controls on a Compound Rotorcraft," AIAA Guidance, Navigation, and Control Conference, Boston, MA, August 19–22, 2013.

[31]Ozdemir, G. T., and Horn, J. F., "Simulation Analysis of a Flight Control Law with In-Flight Performance Optimization," American Helicopter Society 68^{th} Annual Forum, Fort Worth, TX, May 1–3, 2012.

[32]Reddinger, J. P., and Gandhi, F., "A Physics-Based Approach to Trim Optimization of an Articulated Slowed-Rotor Compound Helicopter in High-Speed Flight," American Helicopter Society 70^{th} Annual Forum, Montréal, QC, Canada, May 21–23, 2014.

[33]Saberai, H., Khoshlahjeh, M., Ormiston, R., and Rutkowski, M. "Overview of RCAS and Application to Advanced Rotorcraft Problems," AHS 4^{th} Decennial Specialists' Conference on Aeromechanics, San Francisco, CA, Jan. 21–23, 2004.

[34]Yeo, H., Bousman, W. G., and Johnson, W., "Performance Analysis of a Utility Helicopter with Standard and Advanced Rotors," *Journal of the American Helicopter Society,* Vol. 49, (3), Jul. 2004, pp. 250–270.
doi: 10.4050/JAHS.49.250

[35]Jain, R., Yeo, H., Ho, J. C., and Bhagwat, M. "An Assessment of RCAS Performance Prediction for Conventional and Advanced Rotor Configurations," American Helicopter Society 70^{th} Annual Forum, Montréal, QC, Canada, May 21–23, 2014.